Songklanakarin J. Sci. Technol.
31 (3), 409-417, May - Jun. 2009

Songklanakarin Journal of Science and Technology
http://www.sjst.psu.ac.th

Original Article

Magnetic targeted drug delivery

Timothy Wiedmann*, Yuanyuan Xie and Pengyun Zeng

Department of Pharmaceutics, University of Minnesota,
308 Harvard St. SE, Minneapolis, MN 55455, USA.

Received 17 December 2008; Accepted 20 April 2009

Abstract

Lung cancer is the most common cause of death from cancer in both men and women. Treatment by intravenous or oral administration of chemotherapy agents results in serious and often treatment-limiting side effects. Delivery of drugs directly to the lung by inhalation of an aerosol holds the promise of achieving a higher concentration in the lung with lower blood levels. To further enhance the selective lung deposition, it may be possible to target deposition by using external magnetic fields to direct the delivery of drug coupled to magnetic particles. Moreover, alternating magnetic fields can be used to induce particle heating, which in turn controls the drug release rate with the appropriate thermal sensitive material. With this goal, superparamagetic nanoparticles (SPNP) were prepared and characterized, and enhanced magnetic deposition was demonstrated *in vitro* and *in vivo*. SPNPs were also incorporated into a lipid-based/SPNP aerosol formulation, and drug release was shown to be controlled by thermal activation. Because of the inherent imaging potential of SPNPs, this use of nanotechnology offers the possibility of coupling the diagnosis of lung cancer to drug release, which perhaps will ultimately provide the "magic bullet" that Paul Ehrlich originally sought.

Keywords: aerosol, magnetic targeting, thermal drug release, magnetite

1. Introduction

Magnetic nanoparticles possess several attractive advantages for medical applications, particularly for cancer (Stahlhofen and Moller, 1993; Gupta, 1994; Choi *et al.*, 2004; Duguet *et al.*, 2006; Gupta *et al.*, 2007). First, superparamagnetic nanoparticles (SPNP) are readily detected by magnetic resonance imaging (Stahlhofen and Moller, 1993; Choi *et al.*, 2004). Second, their position can be altered by a non-invasive, external magnetic field gradient (Voltairas *et al.*, 2002; Duguet *et al.*, 2006; Ally *et al.*, 2005). Third, they can be heated with an external alternating magnetic field (Hergt *et al.*, 1988; Pankhurst *et al.*, 2003). Fourth, they have a small, controllable size (Massart, 1981; Gangopadhyay *et al.*, 1992). Fifth, the surface of the nanoparticles can be chemical modified, and ligands can be easily introduced to target the system to specific cells (Gupta, 1994; Gupta *et al.*, 2007). Finally, they do not pose significant safety concerns, because they are composed of simple iron oxides that are biodegradable and have been approved for use as diagnostic agents in imaging the lung (Stahlhofen and Moller, 1993).

The use of magnetic particles for localized therapy was suggested over three decades ago (Widder *et al.*, 1981; Alexiou *et al.*, 2003). Although early efforts with intravenous administration of magnetic particles for liver cancer were disappointing, there is ample proof that magnetic particles can be retained in specific organs with the proper positioning of magnets (Voltairas *et al.*, 2002; Ally *et al.*, 2005; Dames *et al.*, 2007). Our interest in magnetic particles arose from the possibility of further enhancing the selectivity of inhalation drug administration for the treatment of lung cancer. Previously Brain *et al.* (1984), successfully enhanced the deposition of magnetic particles in rabbits using an iron oxide aerosol and external magnetic field gradient. More recently, magnetic aerosol droplets were localized to the upper lobe of a mouse lung thereby demonstrating the potential of

*Corresponding author.
Email address: wiedm001@tc.umn.edu

spatially targeting magnetic aerosols (Dames *et al.*, 2007).

In addition, superparamagnetic particles undergo heating when exposed to an alternating magnetic field, which can be used to prepare thermal sensitive drug delivery systems (Kono, 2001; Peppasand and Leobandung, 2004; Kalambur *et al.*, 2005; Kawai *et al.*, 2005). In general, the response of stimuli responsive delivery systems should be selective to the desired stimulus so that drug release is completely controlled by the stimulus. Another desirable property of these systems is sensitivity, which entails a large change in the rate of drug release with a small change in the environment. The response of the delivery system should also provide a means to control the rate and duration of drug release. Lastly, flexibility to produce a response that is a discrete, discontinuous event at a given stimulus level or the other extreme, in which the response is a continuous increasing function of the stimulus level is desirable. These properties can theoretically be engendered to a drug delivery system with SPNP.

Although studies of thermal sensitive liposomes were promising (Kono, 2001), a more stable alternative is the solid lipid particles (SLNs or lipospheres), which were developed in the mid 1990s. SLNs are particles with a solid lipid matrix and with an average diameter in the nanometer to micrometer range (Mehnertand and Mader, 2001; Wissing *et al.*, 2004; Wong *et al.*, 2007). SLNs are made from lipids, which melt at elevated temperatures, but remain as solids at physiological temperature. Given the many desirable features of SLN, they appear to be a promising platform for drug delivery in conjunction with magnetic particles. This was recognized by Peira *et al.* who introduced superparamagnetic iron oxide nanoparticles into solid lipid particles and found that SLN had slower blood clearance than pure drug (Peira *et al.*, 2003). However, the use of magnetic nanoparticles for both targeting and thermal responsive drug delivery has not been demonstrated in an inhalable drug delivery system. Here, we report the progress towards magnetic deposition of aerosol particles, both *in vitro* and *in vivo* results, and the thermal response/solute release from solid lipid aerosols containing superparamagnetic nanoparticles.

2. Theory

2.1 Deposition of magnetic aerosol particles

Magnetic field gradients create an attractive force on ferromagnetic or paramagnetic particles (Pankhurst *et al.*, 2003; Ally *et al.*, 2005). The magnetic force, F_m, acting on a particle with magnetic moment, m, is:

$$F_m = m(\partial B_z/\partial z) \quad (1)$$

where $\partial B_z/\partial z$ is the z component of the magnetic field gradient. The magnetic moment of the particle is often expressed as the product of the particle volume ($\pi d_p^3/6$), the volume susceptibility, χ_v, and magnetic field strength, H (where B = $\mu_o H$, and $\mu_o = 4\pi \times 10^7$ Tesla/Amp/m and μ_o is the permeability of a vacuum).

The z-component of the induced magnetic field, B_z, is a function of z, which depends on the strength, size, and orientation of the magnet and can be expressed as a function of z as follows

$$(B_z)_{LD} = (\mu_o H/z^n). \quad (2)$$

Taking the derivative and substituting, while also recognizing that the magnetic moment of the particle depends on H, which is also a function of distance, the magnetic force is written as,

$$F_m = (\pi d_p^3/6)\chi_v\mu_o(H/z^n)[\partial(H/z^n)/\partial z] =$$

$$(\pi d_p^3/6)\chi_v\mu_o[(1/2)\partial(H/z^n)^2/\partial z]. \quad (3)$$

The exact functional form of the magnetic field may be determined from experimental measurements or theoretically calculations.

The induced force causes the particle to accelerate, which in turn induces a drag force, F_d, that is dependent on the particle velocity, given by

$$F_d = 3\pi\eta d_p v_z, \quad (4)$$

where η is the viscosity of air (1.8×10^{-5} kg/m.s). The particle quickly reaches a steady state velocity, which may be found by equating the forces, $F_m = F_d$, and solving for the velocity,

$$v_z = dz/dt = \{(d_p^3/12)\chi_v\mu_o^2\partial[(H/z^n)^2]/\partial z\}/(3\pi\eta d_p). \quad (5)$$

This can be integrated if the functional form of magnetic field gradient is known,

$$\int\{\partial[(H/z^n)^2]/\partial z\}dz = +"(d_p^3/12)\chi_v/(18\pi\eta)dt, \quad (6)$$

In general,

$$z = [z_o^{(n+1)} - (n+1)(Kd_p^2)t)]^{(1/(n+1))}, \quad (7)$$

where the value K includes all of the constants. Given the initial distance from the magnet, z_o, the position of the particle at any time, t, along the z-axis may be found. It is noteworthy that for magnetic fields, which decay rapidly with distance (e.g. point dipoles), the large power dependence of the position on magnetic field gradient gives rise to steep particle trajectories near the magnet.

For particle deposition, a simple model is considered that consists of magnetic particles in a cylindrical tube with radius, R, that flow past a wedged-shaped magnetic with its edge positioned along the y-axis, parallel to the tube length. The magnetic field gradient is perpendicular to the direction of the air flow, which in turn is described by Poiseulle's law giving rise to a velocity profile of parabolic shape in the x-z

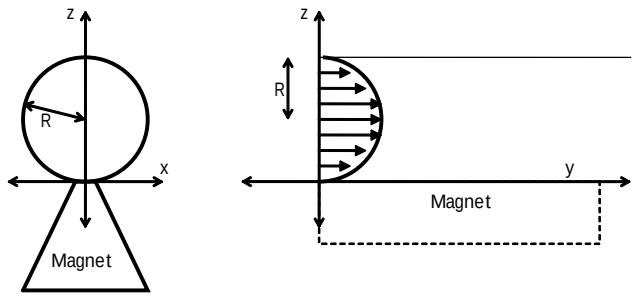

Figure 1. (Left) Magnetic field gradient in a cylindrical tube with radius R

plane. As such, the induced magnetic velocity along z is taken to be independent of the aerodynamic flow along y (Figure 1).

The velocity in the y direction depends on z as

$$v_y = dy/dt = v_m[(2zR\cos\theta - z^2)/R^2], \quad (8)$$

where v_m is the maximum velocity at z = R. The position of the particle along the y-axis at any time can be found by substituting the expression for z (Eqn 8) into Poiseulle's law (Eqn 9) and integrating:

$$\int dy = \int v_m[(2F(H/z)R\cos\theta - ((F(H/z))^2)/R^2]dt. \quad (9)$$

Although the integration and subsequent algebra are tedious, the resulting expression is,

$$y = (v_m/d_p^2K'')\{(1/6)[(z_o^4 - 4d_p^2K''t)^{6/4} - z_o^6] - (2R/5)[(z_o^4 - 4d_p^2K''t)^{5/4} - z_o^5]\}, \quad (10)$$

where K" is a constant incorporating fixed terms and the magnetic field is represented by a line dipole (magnetic field varies with $1/z^2$ and n=4). However, for deposition, the term, $(z_o^4 - 4d_p^2Kt)$, goes to zero, which provides a simple means to calculate the deposition. That is, for an initial z_o that yields a value of y less than the length of the magnet when $(z_o^4 - 4d_p^2 Kt)$ goes to zero, the particle will deposit. If the z_o yields a value greater than the magnet length, the particle is assumed to continue through the tube past the magnet.

2.2 Magnetic hyperthermia

Heating of magnetic particles by an alternating (AC) magnetic field can be understood as follows (Mehnertand and Mader, 2001; Rosensweig, 2002; Peira *et al.*, 2003; Wissing *et al.*, 2004; Kalambur *et al.*, 2005; Wong *et al.*, 2007). Consider a magnetic material located in a magnetic field of strength, where the individual atomic moments in the material contribute to its overall magnetic response, which is known as the magnetic induction, B.

$$B = \mu_o(H+M), \quad (11)$$

where M is the magnetization of the material.

For particles (< 100 nm) with a single magnetic domain, heating by generation of eddy currents in bulk magnetic materials and hysteresis losses in bulk and multi-domain magnetic materials are minor, and relaxation through a Brownian or Néel mechanism dominates the heating (Rosensweig, 2002). In Brownian relaxation, the particle continually rotates towards the changing field direction with its magnetic moment locked along the crystal axis. Heating is caused by the friction between the rotating particle and surrounding fluid. In the Néel mode, the particle is stationary and its magnetic moment rotates towards the changing field and away from the initial easy axis orientation with respect to the crystal. Here, heating is caused by energy released with relaxation as the magnetic moment crosses the effective anisotropy barrier.

Both modes of relaxation are characterized by time constants, τ_N, and τ_B for Néel and Brownian, respectively, which are given by (24),

$$\tau_N = (1/2)\sqrt{\pi}\tau_o \exp(\Gamma)/\Gamma^{1/2}, \quad (12)$$

where the τ_o is of the order of 10^{-9} s, $\Gamma = \kappa V_m/kT$, where κ is the anisotropy constant ($3x10^4$), and V_m is the magnetic volume given by $V_m = \pi d_m^3/6$, and

$$\tau_B = 3\eta V_h/kT, \quad (13)$$

where kT is the product of Boltzmann's constant and absolute temperature, V_h is the hydrodynamic volume given by $V_h = \pi(2\delta + d_m)^3/6$, where δ is the thickness of the adsorbed surfactant layer, and η is the viscosity coefficient of the matrix fluid. Because the two modes take place in parallel, the effective relaxation time, τ, is given by

$$1/\tau = (1/\tau_N) + (1/\tau_B), \quad (14)$$

Therefore qualitatively, smaller particles relax mainly by the Néel mode, while for larger particles, Brownian relaxation dominates.

The volumetric power dissipation, P_{spm}, or specific absorption rate (SAR), is defined as the amount of heat released per unit volume of the material per unit time and is given by (27),

$$P_{spm} = \pi\mu_o\chi H^2 f[2\pi f\tau/(1+2\pi f\tau)^2], \quad (15)$$

where f is the frequency, and χ is the magnetic susceptibility. The heating rate, change in temperature with time, $\Delta T/\Delta t$, for a solution of monodispersed particles is given by

$$\Delta T/\Delta t = P_{spm}C_{sp}, \quad (16)$$

where C_{sp} is the sample-specific heat capacity.

3. Experimental

3.1 Materials

All materials were minimally reagent grade and all solutions were carefully deoxygenated by alternating bubbling with argon and placing under vacuum.

3.2 Preparation of aqueous and coated magnetic nanoparticles

Magnetite nanoparticles were synthesized by chemical coprecipitation of $FeCl_3$ and $FeCl_2$ by the addition of an alkaline solution under an inert atmosphere (Massart, 1981). The reaction consists of the following:

$$Fe^{2+} + 2Fe^{3+} + 8OH^- \rightarrow Fe_3O_4 + 4H_2O$$

The resulting black precipitate was washed and then suspended in 1 mM HCl. This preparation is referred to as the aqueous dispersion of magnetic particles. For coated particles, 0.4ml oleic acid was added and dispersion was heated to 75°C for 30 minutes. The particles were washed with acetone and suspended in cyclohexane. The dispersion was then freeze-dried under high vacuum to produce a dry, black powder.

3.2 Nanoparticle characterization

The composition of coated nanoparticles was determined from the total dry weight and the moles of Fe assayed assuming a molecular formula of $(Fe_3O_4)_x \cdot (C_{18}H_{33}O_2)_y$. The molar concentration of iron was determined using a modified phenanthroline procedure (Rosensweig, 2002). The ratio of iron to oleic acid was determined from the total dry weight and the elemental assay of iron. The induced magnetization and saturation magnetization values of dried Fe_3O_4 were measured with a Vibrating Sample Magnetometer (Lakeshore 7400 Series VSM system, Westerville, OH) at 298 K. The morphology and size of the synthesized particles were observed using transmission electron microscopy (FEI Tecnai T12, Hillsboro, Oregon). The size distribution in water and cyclohexane solution was determined by dynamic light scattering (Nicomp submicron particle sizer, model 370, Pacific Scientific Hiac/Royco Instruments Division, Santa Barbara, CA).

3.3 Aerosol generation and magnetic deposition

An aqueous dispersion was placed in the baffle at the designate concentration, entrained with air and directed into the drying column (Krighna *et al.*, 1970). For ultrasonic generation of coated aerosol particles suspended in cyclohexane, the air was saturated with cyclohexane by an inline bubbler to minimize evaporation. A stainless steel, reflux drying column that had an outer column temperature of 105 or 85°C for the aqueous and cyclohexane dispersions, respectively, and an inner condenser temperature was maintained at 5°C. The resulting dried particles were directed upward through a cylindrical glass tube that had an external, wedged shaped, permanent magnet. Control experiments were conducted in the same manner without the magnet.

The particle deposition fraction was assayed in three different ways. For particles ranging from 100 to 300 nm, a scanning mobility particle (SMPS, TSI, Minneapolis, MN)) analyzer was used. For the size range of 0.5 to 20 μm, an Aerodynamic Particle Sizer® spectrometer (APS™, TSI Incorporated, Model 3321, Shoreview, MN) was used. The deposition of coated particles was also determined by the filter capture method (Whatman International Ltd, Chandler, Arizona) using the phenanthroline assay for iron. The concentration of the magnetite particles in the baffle ranged from 0.75 to 12 mg/ml to produce the desired particle size distribution and mass deposition to yield measurable deposition, and the flow rates were varied between 0.1 and 0.5 LPM, and the tube size ranged from a 1 to 12.7 mm diameter. In addition to the *in vitro* deposition studies, magnetic deposition of coated particles was examined in a mouse model by a nose-only exposure system. Fluorescein was included in the baffle solution and was used as a marker for particle deposition, where the mass of fluorescein in the blood or tissue was determined by HPLC.

3.4 Magnetic heating

Thermal heating was carried out with various amounts of SPNs dispersed in 2 ml cyclohexane or long chain alcohol and placed at the center of a three turn radiofrequency coil (41.5 mm diameter) that generated the AC magnetic field (1 kW Hotshot, Ameritherm Inc., NY). The temperature of the suspending media was measured using a fluoro-optic thermometry system (Luxtron 3100 thermometer, Luxtron Inc., CA). Experiments were carried out at room temperature, and time zero was taken to be when the sample reached 25°C.

4. Results

4.1 SMPS deposition measurements

The aqueous magnetic particle dispersion was used to determine the deposition with the SMPS and APS. The median size of the aqueous dispersion of magnetic particles was 100 to 600 nm depending on storage time. The particles consisted of individual nanoparticles, ca 20 nm diameter, that are aggregated into the larger agglomerate as seen with SEM and TEM images.

From the deposition experiment, the aerosol mass concentration as a function of particle size for the magnet and control is given in Figure 2. The SMPS employs an initial cascade impactor to remove particles that have a geometric size of 500 nm. In the case of the magnetite particles, which

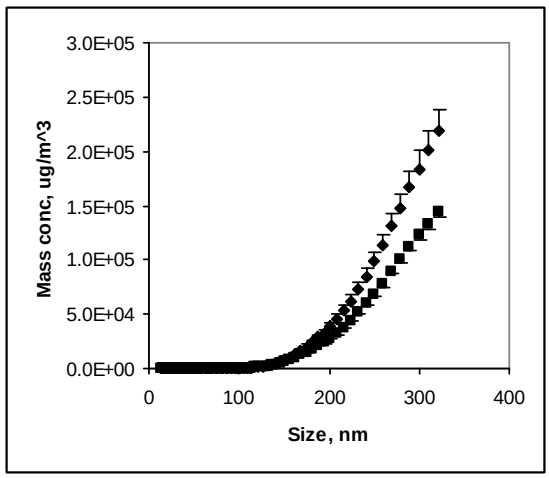

Figure 2. Mass concentration given as a function of particle size for (♦) control and (■) magnetic deposited particles determined at a flow rate of 0.1 LPM and a tube size of 6 mm (od).

were assumed to have a density of 5.18 g/ml, the geometric cutpoint diameter was 322 nm, and only the initial rising portion of the mass distribution can be seen on the SMPS output. Nevertheless, the critical feature is the lower aerosol concentration in the presence of the magnet that reflects the loss due to magnetic deposition on the tube. The data were collected in triplicate with standard deviations at 5% and less.

Also noteworthy in Figure 2 is the divergence of the mass concentration between the magnet group and control as the size increases. The distribution from the magnet group was expressed as a fraction of the control, which was then plotted as a function of particle size. In Figure 3, the deposition fraction is seen to increase with particle size. Comparing the data, the deposition fraction was lower as the air flow rate was increased form 0.1 to 0.3 LPM.

4.2 APS deposition measurements

In a similar manner, the deposition fraction of magnetic particles was determined by the aerodynamic particle sizer (APS), and divergent distributions were seen for the magnet treated and control groups (Figure 4). In Figure 5, the deposition fraction is given as a function of particle size for five air flow rates. As before, the deposition fraction increased with increasing particle size, and consistent with expectations, the deposition fraction for these larger particles was much higher than that seen in the SMPS study. Deposition fractions below 1 ìm tended to be less reliable due to the lower values and inability of laser diffraction methodology to characterize this size range. Here it is also evident that increasing flow rate causes a corresponding decrease in deposition fraction, and there is a dramatic decrease between the 0.1 and 0.2 flow rates, while the change is more regular in progressing to the higher flow rates.

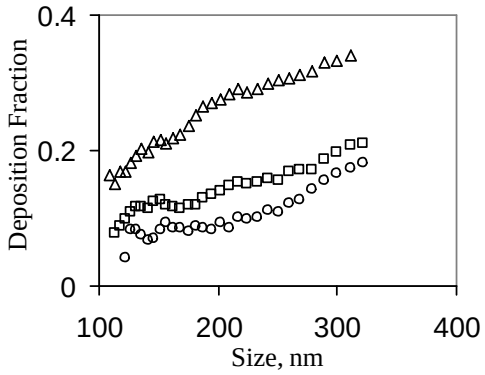

Figure 3. Mean mass deposition fraction as a function of particle size obtained with a 6 mm tube at flow rates of (Δ) 0.1, (□) 0.2 and (O) 0.3 LPM.

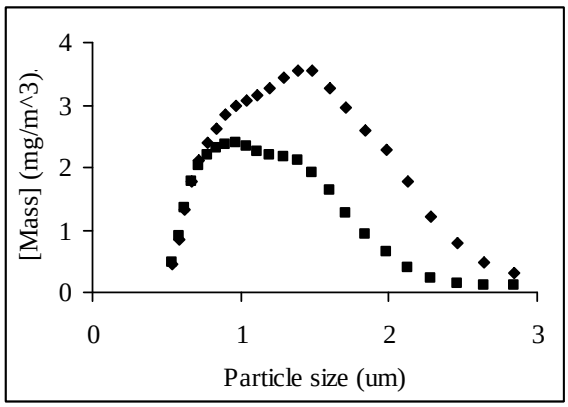

Figure 4. Mass concentration given as a function of particle size for (♦) control and (■) magnetic deposited particles determined at a flow rate of 0.2 LPM and a tube size of 6 mm (od).

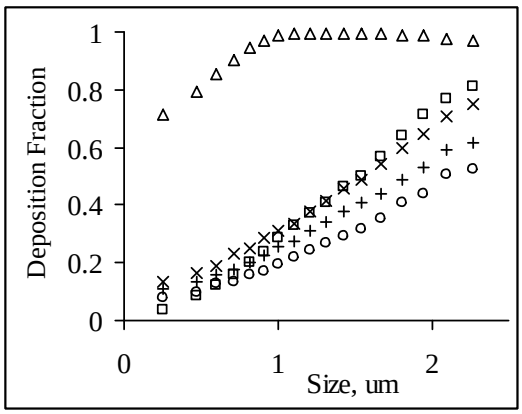

Figure 5. Deposition fraction given as a function of particle size in a 6 mm tube at flow rates of (Δ) 0.1, (□) 0.2, (x) 0.3, (+) 0.4 and (O) 0.5 LPM.

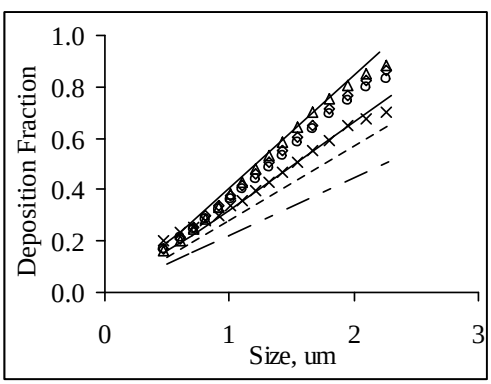

Figure 6. Deposition fraction given as a function of particle size for tube sizes of (Δ) 4, (◊) 6, (O) 8, and (x) 12.7 mm (id) using a flow rate of 0.2 LPM. The lines represent simulated deposition fractions assuming a line dipole function for the permanent magnet.

The effect of tube size was also examined as shown in Figure 6. As the tube size was increased from 4 to 12.7 mm, lower deposition fractions were observed, although there remained a linear dependence on the particle size. The lines shown on the figure represent simulations from a model where the magnetic field was assumed to be represented by a line dipole, $B = f(H/z^2)$.

4.3 Characterization of coated particles

For the magnetic deposition of the coated particles, which would represent a more practical material for a drug delivery system than the aqueous dispersion used above, an initial thorough characterization was carried out. Complexation with phenanthroline was used to measure the iron content that is independent of its oxidation state. From control assays, the slopes and intercepts of standard curves composed of $FeCl_2$, $FeCl_3$, Fe_2O_3, and Fe_3O_4 were statistically indistinguishable with molar absorptivities based on iron content were near 11,560 A $M^{-1}cm^{-1}$, which is in good agreement with the literature value of the ferrous complex, given at 11,100 $M^{-1}cm^{-1}$ (24). The oleic acid content of the synthesized particles by weight was determined to be 23.8± 1.4 %, 26.6±4.3 %, and 26.2±2.6 %, and the synthetic yield based on iron was 77%. From TEM, the particles appeared in an aggregated state, but individual particles with a diameter nearly 20 nm and smaller were clearly seen. Given the particle size, the oleic acid content is consistent with a monolayer of coverage on each 20 nm particle.

The induced magnetic moment was determined as a function of applied field that was varied between -15,000 and +15,000 Gauss, resulting in an induced field that ranged between -50 and +50 emu/g. The induced moment was reversible, and no hysteresis was observed characteristic of superparamagnetic nanoparticles. The maximum induced magnetization was calculated from the values at the plateau of the plot and was 54 emu/g.

4.4 Magnetic deposition

The tabular values for the deposition fractions for the coated particles are given in Table 1 along with the aerodynamic diameter. The particle size distributions at the lower concentrations were unimodal, but with the higher concentrations two peaks were evident with the modes occurring on the stages with cutoff diameters of 0.59 and 1.21 μm. The fitted aerodynamic diameter, assuming unimodal behavior, increased with increasing concentration. For the three lower concentrations, the mass median aerodynamic diameter (MMAD) increased as expected in a linear manner with the cube root of the baffle concentration. However, at 6 and 12 mg/ml, the size was smaller than expected.

In contrast to the SMPS and APS results, the deposition fraction did not increase in a linear manner with particle size (Table 1). This is possibly due to aggregation of the particles and polydispersity of the aerosol. As previously seen, increasing flow rate lead to a decrease in the deposition fraction. With respect to tube size, high deposition fractions were observed for the two smaller tubes (1 and 2 mm), but similar fractions were observed for the four larger sizes of 4 to 12.7 mm.

4.5 *In vivo* magnetic deposition

A nose only deposition study was carried out in the mouse with dried aerosol droplets that contained fluorescein and coated magnetic particles. Following a 5 min exposure,

Table 1. Effect of aerosol mass median aerodynamic diameter and geometric standard deviation (MMAD±GSD) on deposition fraction (mean±SD) determined in a 6 mm tube at an air flow rate of 0.2 LPM.

MMAD (μm) ± GSD	Aerosol Conc, ug/L	Deposition fraction
0.61±1.80	61±4.6	0.249±0.026
0.80±1.94	178±13	0.302±0.041
0.97±1.91	384±30	0.375±0.030
1.01±2.01	665±11	0.478±0.080
1.07±2.03	1447±87	0.595±0.039

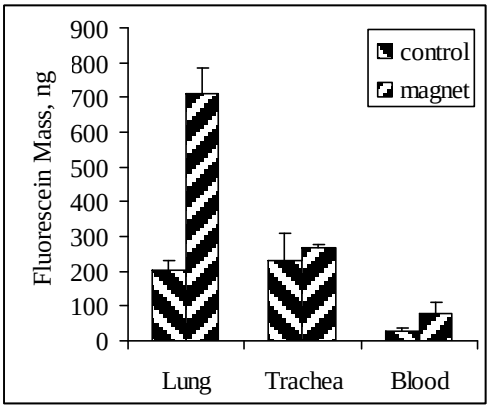

Figure 7. Mass of fluorescein (mean ± SD, n=3) deposited in the lung (below carina), trachea and blood with coated magnetic aerosol particles in mouse model in the presence (magnet group) and absence (control) of wedge-shaped magnet using a nose only exposure system.

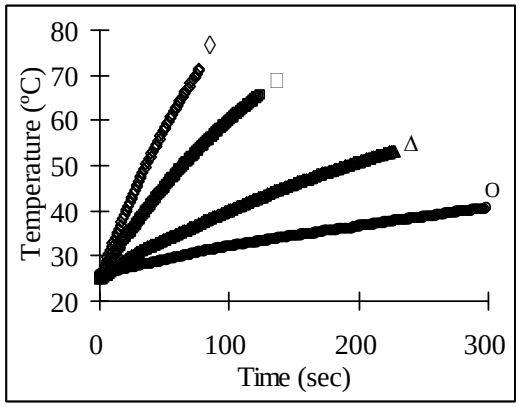

Figure 8. Temperature of SPNs in cyclohexane as a function of time for concentrations of (O) 0.625, (Δ) 5, (□) 10, and (◊) 20 mg/ml at magnetic field H = 6.0 kA/m and frequency f = 386 kHz.

the mice were sacrificed and the lung, trachea, and blood samples were obtained and analyzed for fluorescein by HPLC. The assayed mass for each tissue obtained with the magnet treated and control are given in Figure 7. The mass deposited in the lung with the magnet was over three times greater relative to the control. The trachea and blood levels were also higher, but difference for the trachea failed to reach statistical significance. Nevertheless, enhanced magnetic deposition was clearly demonstrated with the use of coated magnetic particles.

In summary, *in vitro* measurements and modeling of the magnetic deposition of aerosol particles has been carried out. With further analysis, the functional dependence of the deposition on the critical parameters (particle size, air flow rate, tube geometry, and particle magnetic moment) can be used to identify the necessary properties/limitations for magnetic deposition of aerosol particles in humans. In addition, magnetic field shape and strength can be evaluated to optimize the spatial selectivity of the aerosol deposition.

4.6 Magnetic particle heating

The second aspect of the research study involved measurement and theoretical evaluation of the heating of superparamagnetic particles. For SPNs dispersed in cyclohexane at concentrations ranging from 0.625 to 20 mg/ml, the temperature is plotted as a function of time, where the frequency was 386 kHz and the magnetic field strength was 6.0 kA/m (Figure 8). The temperature increased with time in a nonlinear manner and to facilitate comparison, the data were fit to a polynomial function, and the linear term is given in Table 2.

The initial heating rate increased from 0.0098 to 0.15 at 3.5 kA and 0.033 to 0.717°C/s at 6.0 kA in an apparently linear manner with particle concentration. The heating rates were calculated using Equations 15 and 16, and generally, the observed rates are very close to the calculated values with none differing by more than 25%. This is perhaps more remarkable, recognizing that neither the polydispersity of the particles nor the change in viscosity with time was considered. Additional studies were carried out at frequencies of 190, 268, and 386 KHz, which were also in agreement with theoretical predictions.

The heating response of SPNs when dispersed in cetyl alcohol, which melts over a broad range beginning at 49°C, was then determined. Figure 9 shows the temperature

Table 2. Observed heating rate of SPNs compared with heating rate from modeling calculation in cyclohexane at the indicated field strengths and a frequency 386 kHz.

Particle concentration (mg/ml)	Observed heating rate (°C/s)	Heating rate from model (°C/s)	Observed heating rate (°C/s)	Heating rate from model (°C/s)
	3.5 kA		6.0 kA	
0.625	0.0098	0.0082	0.0330	0.0227
2.5	0.0391	0.0326	0.1153	0.0909
10	0.1499	0.1304	0.4443	0.3631

as function of time for three particle weight percents, 5%, 25% and 33%, using a 6 kA/m magnetic field at 386 kHz. For the lowest concentration, the sample temperature increased in a manner similar to that seen for cyclohexane. At the two higher particle concentrations, the profiles were distinct, and their appearance reflects the change in the state (i.e. melting) of the cetyl alcohol. In the first phase (25-45°C) when the particles are dispersed in the solid cetyl alcohol, the temperature increase profile was comparable to those above. In the second phase (45~49°C), when the temperature approaches the melting point of cetyl alcohol, the rate of temperature increase was much lower, which is consistent with enthalpic heating demands of cetyl alcohol melting. Following completing of the melting, the heating rate again increases. The results for the thermal changes in a lipid matrix, phase changes have been achieved that are adequate for controlling drug release. Moreover, these changes have been achieved using a realistic SPN load ($\leq$33%) and readily accessible field strengths and frequencies.

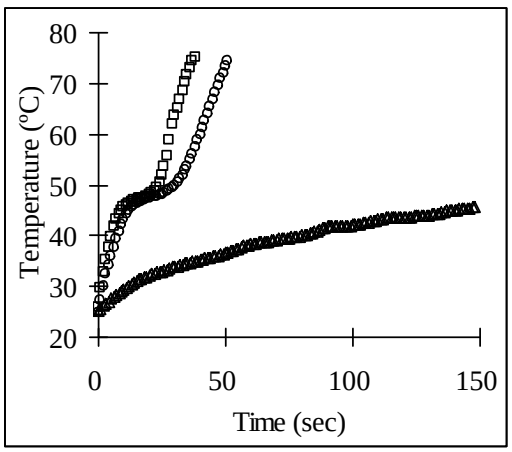

Figure 9. Temperature of SPNs in cetyl alcohol as a function of time for three different concentration at magnetic field H = 6.0 kA/m and frequency f = 386 kHz.

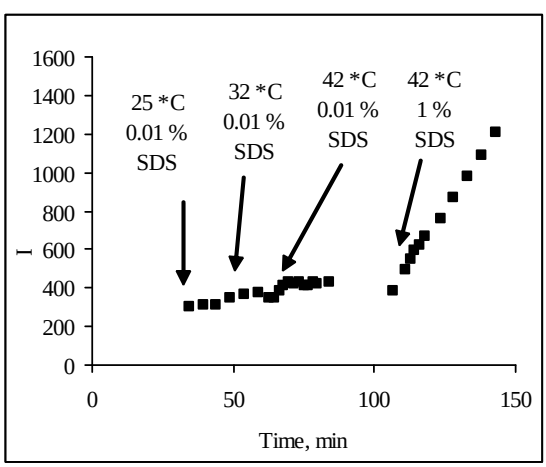

Figure 10. Fluorescent intensity of diphenyl hexatriene (proportional to released solute concentration) given as a function of time for indicated media composition and temperatures.

5. Summary and Conclusions

In summary, we have demonstrated that solute release can be controlled by melting of a lipid matrix using SLN that have a respirable particle size (1 μm). Overall, the deposition of magnetic aerosol particles, the thermal activation, and solute release from a solid lipid particle of respirable size have been demonstrated. These features represent the essential aspects in demonstrating the feasibility of SPN/SLN as a thermal responsive drug delivery system for inhalation.

References

Alexiou, C., Jurgons, R., Schmid, R.J., Bergemann, C., Henke, J., Erhardt, W., Huenges, E. and Parak, F. 2003. Magnetic drug targeting - Biodistribution of the magnetic carrier and the chemotherapeutic agent mitoxantrone after locoregional cancer treatment. J Drug Target 11(3), 139-149.

Ally, J., Martin, B., Behrad Khamesee, M., Roa, W. and Amirfazli, A. 2005. Magnetic targeting of aerosol particles for cancer therapy. J Magn Magn Mat 293 (1), 442-449.

Brain, J.D., Valberg, P.A. and Gehr, P. 1984. Correlation between the behavior of magnetic iron oxide particles in the lungs of rabbits and phagocytosis. Exp Lung Res 6(2), 115-31.

Choi, H., Choi, S.R., Zhou, R., Kung, H.F. and Chen, I.W. 2004. Iron oxide nanoparticles as magnetic resonance contrast agent for tumor imaging via folate receptor-targeted delivery. Acad Radiol 11(9), 996-1004.

Dames, P., Bernhard, G., Flemmer, A., Hajek, K., Seidl, N., Wiekhorst, F., Eberbeck, D., Bittmann, I., Bergemann, C., Weyh, T., Trahms, L., Rosenecker, J. and Rudolph, C. 2007. Target delivery of magnetic aerosol droplets to the lung. Nature Nanotechnology 2, 495-499.

Duguet, E., Vasseur, S., Mornet, S. and Devoisselle, J.M. 2006. Magnetic nanoparticles and their applications in medicine. Nanomed 1(2), 157-168.

Gangopadhyay, S., Hadjipanayis, G.C., Dale, B., Sorensen, C.M., Klabunde, K.J., Papaefthymiou, V. and Kostikas, A. 1992. Magnetic-Properties of Ultrafine Iron Particles. Phys Rev B 45(17), 9778-9787.

Gupta, A.K., Naregalkar, R.R., Vaidya, V.D. and Gupta, M. 2007. Recent advances on surface engineering of magnetic iron oxide nanoparticles and their biomedical applications. Nanomed 2 (1), 23-39.

Gupta, P.K. 1994. Magnetically controlled targeted chemotherapy. In Willmott N and Daly J (eds) Microspheres and regional cancer therapy (CRC Press, Boca Raton Fl), 71-116.

Hergt, R., Andra, W., d'Ambly, C., Hilger, I., Kaiser, W., Richter, U. and Schmidt, H. 1988. Physical limits of

hyperthermia using magnetite fine particles. IEEE Trans. Magn, 34, 3745-54.

Kono, K. 2001. Thermosensitive polymer-modified liposomes. Adv Drug Deliv Rev 53, 307-19.

Kalambur, V.S., Han, B., Hammer, B.E., Shield, T.W. and Bischof, J.C. 2005. In vitro characterization of movement, heating and visualization of magnetic nanoparticles for biomedical application, Nanotechnology 16, 1221-1233.

Kawai, N., Ito, A., Nakahara, Y., Futakuchi, M., Shirai, T., Honda, H., Kobayashi, T. and Kohri, K. 2005. Anticancer effect of hyperthermia on prostate cancer mediated by magnetite cationic liposomes and immune-response induction in transplanted syngeneic rats. Prostate 64, 373-81.

Krighna, G.S.R., Murti, M.A. and Sarmk, V.A.K. 1970. Spectrophotometric Determination of Iron with Orthophenanthroline. Microchemical Journal 15, 585-589.

Liao, X.M., Liang, W. and Wiedmann, T. 2004. Lung distribution of the chemopreventive agent difluoromethylornithine (DFMO) following oral and inhalation delivery. Exp Lung Res 30(8), 755-769.

Massart, R. 1981. Preparation of Aqueous Magnetic Liquids in Alkaline and Acidic Media. IEEE Trans Magn 17(2), 1247-1248.

Mehnertand, W. and Mader, K. 2001. Solid lipid nanoparticles: production, characterization and applications. Adv Drug Deliv Rev 47, 165-196.

Pankhurst, Q.A., Connolly, J., Jone, S.K. and Dobson, J. 2003 Applications of magnetic nanoparticles in biomedicine. J. Phys. D: Appl. Phys 36, 167-81.

Peira, E., Marzola, P., Podio, V., Aime, S., Sbarbati, A. and Gasco, M.R. 2003. In vitro and in vivo study of solid lipid nanoparticles loaded with superparamagnetic iron oxide. J Drug Target 11, 19-24.

Peppasand, N.A. and Leobandung, W. 2004. Stimuli-sensitive hydrogels: ideal carriers for chronobiology and chro-notherapy. J Biomater Sci Polym Ed 15, 125-44.

Rosensweig, R.E. 2002. Heating magnetic fluid with alternaing magnetic field. J Magn Magn Mat 252, 370-374.

Stahlhofen, W. and Moller, W. 1993. Behaviour of magnetic micro-particles in the human lung. Radiat Environ Biophys 32(3), 221-238.

Voltairas, P.A., Fotiadis, D.I. and Michalis, L.K. 2002. Hydrodynamics of magnetic drug targeting. J Biomech 35(6), 813-821.

Widder, K.J., Morris, R.M., Poore, G., Howard, D.P., Jr. and Senyei, A.E. 1981. Tumor remission in Yoshida sarcoma-bearing rts by selective targeting of magnetic albumin microspheres containing doxorubicin. Proc Natl Acad Sci U S A 78(1), 579-581.

Wissing, S.A., Kayser, O. and Muller, R.H. 2004. Solid lipid nanoparticles for parenteral drug delivery. Adv Drug Deliv Rev 56, 1257-1272.

Wong, H.L., Bendayan, R., Rauth, A.M., Li, Y. and Wu, X.Y. 2007. Chemotherapy with anticancer drugs encapsulated in solid lipid nanoparticles. Adv Drug Deliv Rev 59, 491-504.